Algorithm Description Document for Version 3.1 of the Three-Dimensional Gridded NEXRAD WSR-88D Radar (GridRad) Dataset

Last Revised: 28 August 2017

Revision History:

- 28 August 2017 - Original release.

Author Information:
Cameron R. Homeyer*
School of Meteorology
University of Oklahoma
Norman, OK 73072-7307
Contact: chomeyer@ou.edu

Kenneth P. Bowman
Department of Atmospheric Sciences
Texas A&M University
College Station, TX 77843-3150
Contact: k-bowman@tamu.edu

*Primary scientific contact.

Table of Contents

1 Introduction

1.1 Objective

The objective of this document is to describe the algorithms used to produce Version 3.1 of the three-dimensional Gridded NEXRAD WSR-88D Radar data. This data set is referred to as *GridRad*. Additional information is available at GridRad.org. The GridRad data are available for download from the Research Data Archive of the National Center for Atmospheric Research as dataset ds841.0.

1.2 Scope

The scope of this document is a detailed outline of the characteristics of NEXRAD WSR-88D Level 2 (i.e., native volume scan) data, the computational steps used to merge Level 2 data onto large-area grids, and recommended use of the GridRad data produced by these methods. Individuals may leverage the detail within this document to reproduce the GridRad methods or reference it when analyzing the publicly available dataset to ensure proper scientific understanding and evaluation. Example code for reading and quality controlling GridRad data is also provided.

2 NEXRAD WSR-88D Data

The U.S. operational weather radar system, now known as the Next Generation Weather Radar (NEXRAD) program, was created in 1957. Beginning in 1988, the network was upgraded to Doppler S-band (10–11.1 cm wavelength) horizontal-polarization radars (Weather Surveillance Radar 1988 Doppler or WSR-88D) to measure the radial velocity V_{R} and the velocity spectrum width σ_{V} in addition to the radar reflectivity factor Z_{H} (Crum and Alberty, 1993). From 2011 to 2013, the WSR-88D systems were further upgraded to obtain measurements at both horizontal (H) and vertical (V) polarization. The added polarimetric variables are the differential radar reflectivity Z_{DR}, the differential propagation phase shift ϕ_{DP}, and the co-polar correlation coefficient ρ_{HV}. The polarimetric variables provide information on the size, shape, and concentration of hydrometeors. There are now 143 operational WSR-88D radars in the contiguous U.S. (CONUS) providing nearly continuous coverage of storm systems and their microphysical characteristics. Figure 1 shows the locations of these radars and their combined coverage at the lowest scanned altitudes.

Data from operational NEXRAD WSR-88D radars are archived at the National Centers for Environmental Information (NCEI, formerly the National Climatic Data Center) and Amazon Web Services (AWS) for the period from 5 June 1991 to the present, although data availability for most current systems in the network begins in 1995. The archives include the native three-dimensional data from each radar system (Level 2 data), which are provided on a spherical grid (azimuth, elevation, and range) with its origin at the radar location. Observations from individual systems are subject to some outages and interruptions, but these are typically limited to a few days each year. In general, data gaps are more frequent during years prior to 2005.

The resolution of each radar observation depends on the operating mode (meteorological target) and year. In particular, the number of elevation angles in a volume can be as high as 14 for convection and as low as 5 for clear air or shallow precipitating systems. Select combinations of elevation angles are referred to as Volume Coverage Patterns (VCPs), with each unique VCP accompanied by a number code. Convection is typically sampled using VCP-11 or VCP-12 (or one of their derivatives), both of which contain 14 elevation angles. VCP-12 is often the preferred VCP for convection in recent years. Winter storms (or other shallow precipitation) are typically sampled using VCP-21 (or one of its derivatives), which contains 9 elevation angles. The elevation angles typical of these three VCPs are provided in Table 1. For more information on NEXRAD scanning strategies and characteristics, the reader is directed to Part C of the Office of the Federal Coordinator for Meteorology (OFCM) Federal Meteorological Handbook No. 11 (OFCM, 2006).

Operating Mode	**Elevation angles** (°)
VCP-11	0.50, 1.45, 2.40, 3.35, 4.30, 5.25, 6.20, 7.50, 8.70, 10.0, 12.0, 14.0, 16.7, 19.5
VCP-12	0.50, 0.90, 1.30, 1.80, 2.40, 3.10, 4.00, 5.10, 6.40, 8.00, 10.0, 12.5, 15.6, 19.5
VCP-21	0.50, 1.45, 2.40, 3.35, 4.30, 6.00, 9.00, 14.6, 19.5

Table 1: Elevation angles of the three most common VCPs employed when NEXRAD WSR-88D radars sample precipitation: VCP-11, VCP-12, and VCP-21.

Data storage requirements for NEXRAD data have changed over time due to changes in the spatial grid resolution and the introduction of new measurement variables. Data from the period prior to May of 2008 are stored at an azimuthal resolution of 1° and a range resolution of 1 km. Beginning in May of 2008 the radars transitioned to a range resolution of 250 m and an azimuthal resolution of 0.5° for the lowest 3-5 elevations (referred to as "super-resolution"). Similarly, the addition of polarimetric variables has increased the volume of archived data. A single WSR-88D volume scan of deep convection prior to 2008 includes

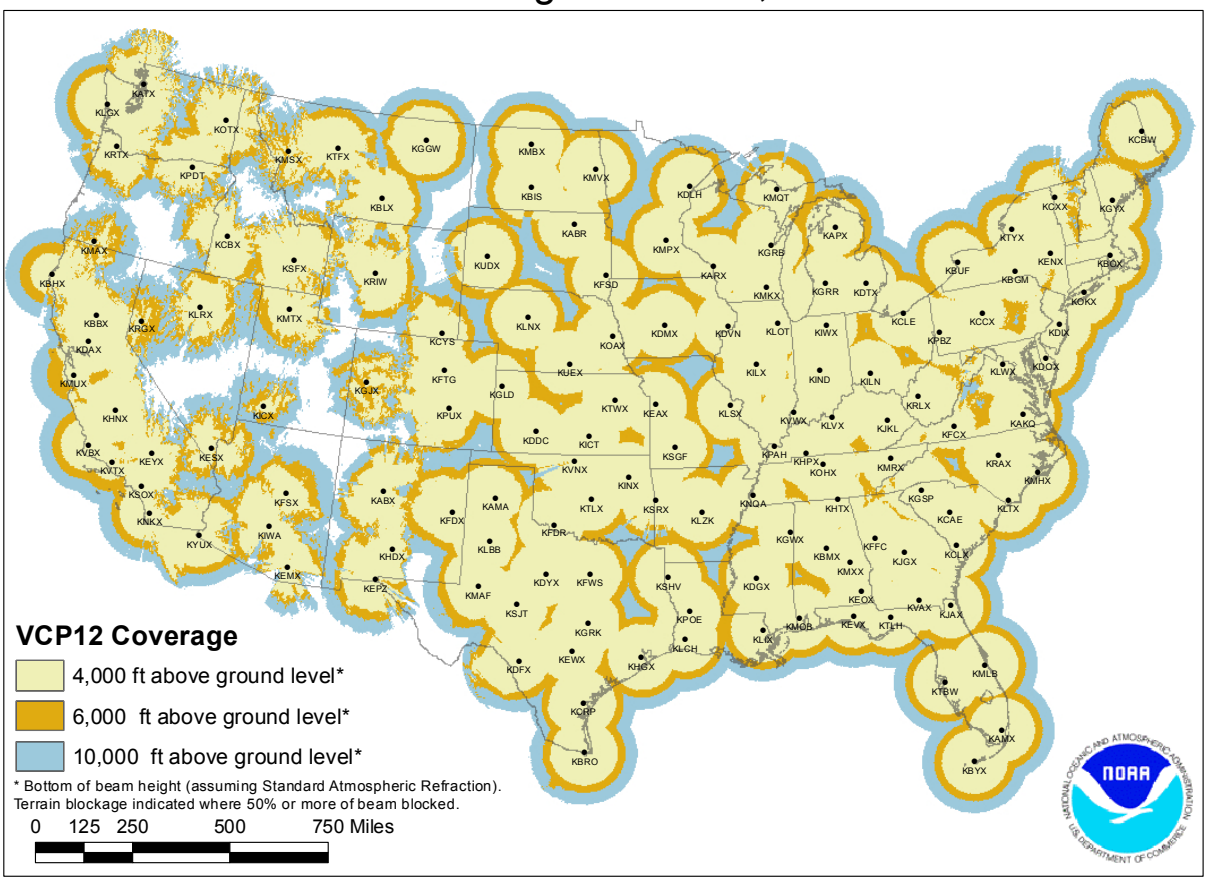

Figure 1: Map of NEXRAD WSR-88D radars within the CONUS and their lowest sampled altitudes for only those altitudes less than 10,000 ft AGL (∼3 km). Credit: NOAA, available online at https://www.roc.noaa.gov/WSR88D/Maps.aspx.

only three variables (Z_{H}, V_{R}, and σ_{V}) on the coarser spherical grid (1 deg × 1 km × 14 elevations) and has a file size of ∼15 MB. In comparison, a similar current observation with the additional polarimetric variables (Z_{DR}, ϕ_{DP}, and ρ_{HV}) on the higher-resolution spherical grid has a file size of ∼45 MB, which is a factor of 3 larger than the earlier files. As a result of the large data volume, data storage and handling is a significant challenge for studies of longer periods. For example, the CONUS region used for GridRad Version 3.1 includes 125 radars and requires ∼5 TB of data storage for a single year prior to 2008 and about four times as much per year for recent years.

Several previous efforts have attempted to improve the utility of NEXRAD data by merging observations from multiple radars onto three-dimensional Earth-referenced grids (typically longitude, latitude, and altitude; hereafter 'gridded' data). This can reduce storage requirements and make the data easier to use. The overlapping observations from multiple NEXRAD WSR-88D radars also allow for a three-fold increase in vertical sampling compared to an individual radar (i.e., the Δz is reduced from 3 km on average to less than 1 km), which provides an important improvement in the utility of NEXRAD data for research. For example, Figure 2 shows the combined vertical sampling in altitude layers of 0-10 km and 0-20 km ASL

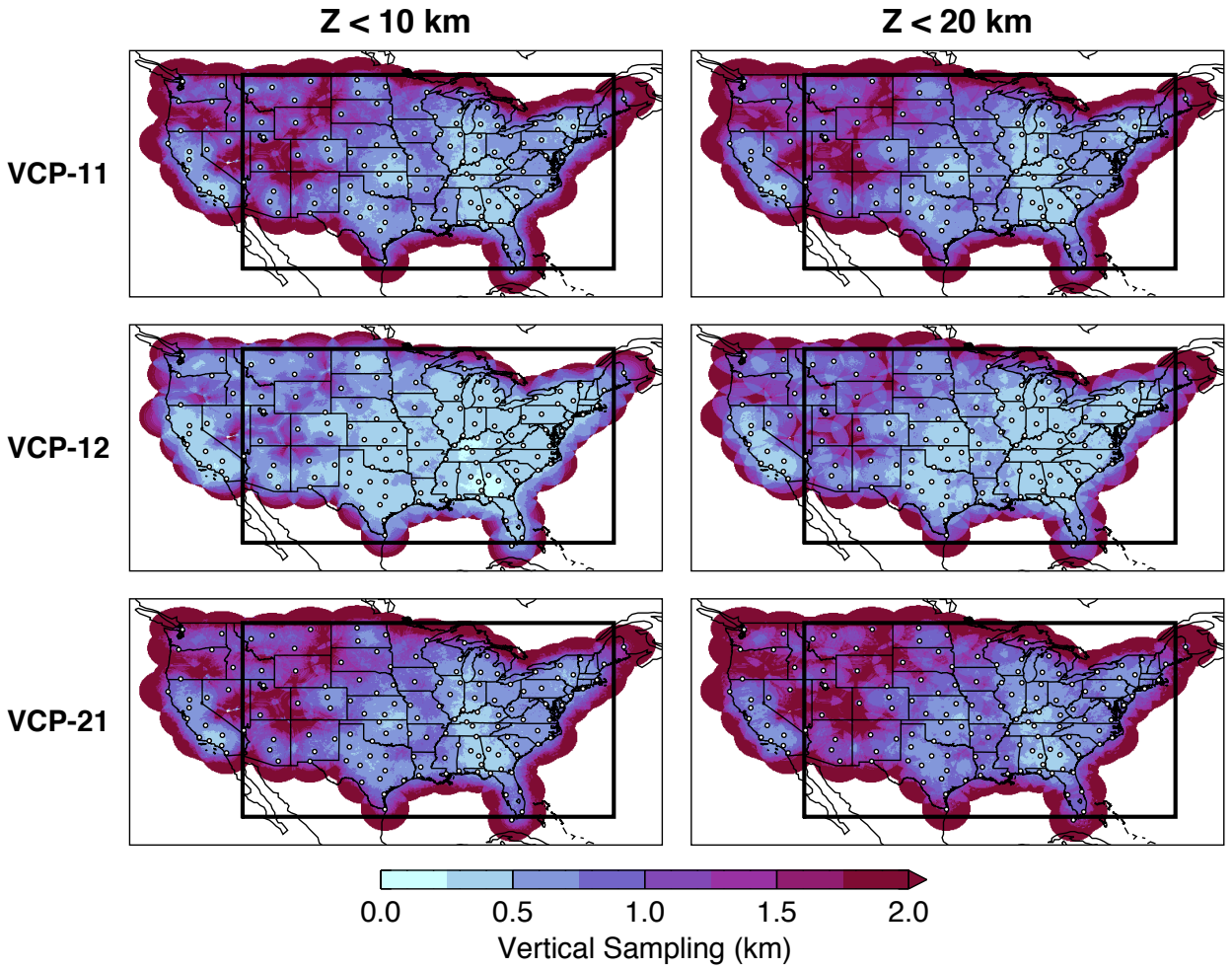

Figure 2: Maps of the combined vertical sampling of merged radar volumes using data out to 300 km in range from radars within the NEXRAD WSR-88D network. The left and right columns show average vertical sampling within the 0-10 km and 0-20 km ASL altitude layers, respectively. Vertical sampling is computed assuming all contributing radars are operating in (top) VCP-11, (middle) VCP-12, and (bottom) VCP-21. The locations of individual radars (white dots) and the GridRad domain (thick black box) are superimposed.

from merging of NEXRAD WSR-88D Level 2 data assuming individual radars are operating in each of the three typical VCPs, as outlined above. These improvements in the utility of NEXRAD data through multi-radar merging motivate the development of the GridRad dataset. The following section outlines the methods employed to create GridRad data.

3 GridRad Algorithm

3.1 Overview

Merging individual NEXRAD WSR-88D volumes onto a common large-area grid can be a somewhat complicated process that depends on the radar variable being merged and its intended use when complete. Established alternative approaches to that outlined here exist, such as those employed in the Multi-Radar, Multi-Sensor (MRMS) system produced within the National Severe Storms Laboratory (NSSL; http://www.nssl.noaa.gov/projects/mrms/). This section is meant to outline the common steps in merging any radar variable in the GridRad dataset.

In the following we distinguish between the observations from a single radar, which are made on a spherical polar coordinate grid with the radar located at the origin, and the GridRad data, which are defined on a regular longitude-latitude-altitude grid. A *Level 2 radar volume* is an observation made by a single radar at a given azimuth, elevation, and range or 'gate'. A *GridRad volume* is a rectangular volume in longitude, latitude, and altitude[1]. The GridRad analysis domain extends from 245°E to 295°E (155°W to 69°W) longitude, 25°N to 49°N latitude, and 1 to 24 km in altitude ASL. The grid resolution is 0.02° longitude × 0.02° latitude × 1 km altitude (∼1.5 km × ∼2 km × 1 km). The centers of the GridRad volumes (x_i, y_j, z_k) are given by

$$\begin{aligned} x_i &= 245 + 0.02\,i, & i &= 0, ..., 2300 \\ y_j &= 25 + 0.02\,i, & j &= 0, ..., 1200 \\ z_k &= 1 + k, & k &= 0, ..., 23, \end{aligned} \tag{1}$$

where x_i is longitude in degrees east, y_j is latitude in degrees north, and z_k is altitude in km. The GridRad grid has 2301 × 1201 × 24 grid points (∼66 million points).

The GridRad algorithm is a four-dimensional binning (averaging) procedure that merges multiple Level 2 radar volumes to estimate radar variables within the GridRad volumes at synoptic analysis times. The Level 2 observations are weighted by their distance from the radar and by the time difference between the observation and analysis times. GridRad Version 3.1 analyses are made hourly from 00 to 23 UTC.

These characteristics describe the hourly GridRad archive publicly available on NCAR's Research Data Archive. It is possible to create GridRad data on any domain within the CONUS using a time resolution of the user's choice. In fact, the authors often create analyses at 5 min intervals for case studies. It is recommended, however, that such data be created using an equivalent spatial resolution to that used in the public archive.

3.2 Procedure

Creation of GridRad data follows a 4-step procedure that is repeated for each contributing Level 2 volume:

1. Read NEXRAD WSR-88D Level 2 observation in polar coordinates (i.e., azimuth, elevation, and range relative to the radar location).
2. Identify common grid volumes in which to bin Level 2 observations.
3. Compute space-time weights of each Level 2 polar grid volume.
4. Bin radar variable(s) scaled by space-time weights into common grid.

[1]Technically the GridRad volumes are defined in Earth-centered spherical polar coordinates. Because the dimensions of a grid box are small compared to the radius of the Earth, the individual grid volumes are effectively rectangular.

Note: Steps 2-4 are carried out for each azimuthal sweep (i.e., 360° scan at a single elevation) of a Level 2 volume and Step 4 is repeated for an azimuthal sweep when more than one radar variable is binned into the common grid (e.g., Z_{H} and the polarimetric variable Z_{DR}). Each step is outlined in the following paragraphs.

Step 1. Read NEXRAD WSR-88D Level 2 observation in polar coordinates.

As outlined in Section 2, the characteristics of the NEXRAD WSR-88D Level 2 data have changed considerably over time, including the resolution of the polar grid, the scan strategy (i.e., vertical sampling), and the radar variables observed. These changes affect the quality of the data beyond that due to the pulse frequency and power of the radar beam, which are often the most important elements to consider when merging multiple radars onto a common grid. In particular, the maximum unambiguous range of a NEXRAD WSR-88D radar depends on the variable observed and transmitted pulse repetition frequency. V_{R} and σ_{V} are only observed out to 230 km in range in the older, lower resolution Level 2 data and out to 300 km in range in the more recent, higher resolution volume scans (i.e., since mid-2008). On the other hand, Z_{H} is observed out to 460 km in range throughout time. The polarimetric variables (Z_{DR}, ϕ_{DP}, and ρ_{HV}), available from all NEXRAD WSR-88D radars since early 2013, are observed out to 300 km in range.

Considering the above limitations of NEXRAD WSR-88D sampling and the goal of a merged dataset to improve spatial coverage from the overlapping of neighboring radars, only observations out to 300 km in range from each radar and within 3.8 min of the analysis time are merged by the GridRad procedure. The time limit is imposed to prevent excessive smoothing of GridRad data. A $\pm$3.8 min window corresponds to a time weighting value of 0.1 (see Step 3 below). The longitude, latitude, and altitude relative to the geoid are computed for each Level 2 radar volume using simple geometry that accounts for the spherical shape of the Earth and assumes the standard index of refraction for the atmosphere in the vertical (e.g., see Chapter 2 in Doviak and Zrnić, 1993). The central time of each azimuthal sweep is used for binning purposes. (Azimuthal sweeps are typically completed in $\sim$20 s by NEXRAD radars when sampling precipitation). To ensure that all usable data are included, all Level 2 volume scans within a $\pm$10 min window of the GridRad analysis time are examined for azimuthal sweeps that fall within the $\pm$3.8 min time window.

Step 2. Identify Level 2 radar volumes that contribute to each common grid volume.

The Earth-referenced coordinates computed in Step 1 are used to find the radar volumes that contribute to each GridRad grid volume. Because the NEXRAD WSR-88D beam is conical, with an average angular beam width of 0.95°, the volume observed by the radar increases with range. In the horizontal, Level 2 radar volumes are assumed to contribute only to the nearest GridRad column. In altitude, each Level 2 radar volume may contribute to more than one GridRad volume, depending on range from the radar. The beam width is taken to be the full width at half maximum power of the transmitted beam. Thus, despite the increasing size of the radar beam with increasing range, the majority of the returned power comes from targets near the beam center (e.g., a collection of precipitation-sized hydrometeors). This results in relatively small differences in the radar variables when measured at small and large distances from a radar, as long as the scatterers are somewhat homogeneous within the field of view (e.g., see Figure 5 in Homeyer (2014)). Nevertheless, it is not appropriate to treat observations made at significantly different ranges from a radar equivalently when merging data onto a common grid. While this treatment is primarily handled through weighting of the individual Level 2 radar volumes in space and time (see Step 3 below), we also set an upper limit to altitude assignments of the beam in the averaging procedure. In particular, we do not allow an individual Level 2 radar volume to contribute to a depth larger than 1.5 km in the common grid (up to three 1-km grid volumes). This limit reduces the potential contribution of radar observations beyond a range of

~90 km (i.e., the point at which the NEXRAD WSR-88D beam depth – and similarly, width – reaches 1.5 km). This restriction prevents excess smoothing of the GridRad data from observations made at far ranges, which can lead to both the loss of important detail from contributing observations at smaller ranges from a radar and an exaggeration of the spatial extent of echo.

Step 3. Compute space-time weights of each Level 2 polar grid volume.

The approach of distance-weighting has been explored in previous studies that merge individual radar volumes onto a common grid and is used primarily to retain spatial scales that are adequately sampled from one radar while preventing retention of corresponding observations from additional radars that are under-sampled (e.g., Trapp and Doswell, 2000; Zhang et al., 2005; Langston et al., 2007). Such an approach is also employed in the GridRad algorithm via a Gaussian scheme in space and time. The weight w is

$$w(r,t) = e^{-r^2/L^2} e^{-\Delta t^2/\tau^2} \ , \tag{2}$$

where r is the radial distance of the polar grid volume from the radar location in kilometers, Δt is the time difference between the observation and GridRad analysis time in seconds, L = 150 km is the spatial scale, and τ = 150 s is the time scale. Figure 3 shows this weighting function out to 300 km in range from a radar and 300 s in time from the GridRad analysis. Sensitivity tests (not shown) demonstrate that changes in the internal microphysical characteristics of a storm from varying L or τ are minimal for values less than 150 km (or s), while values significantly greater than these thresholds show much less detail (i.e., excessive smoothing).

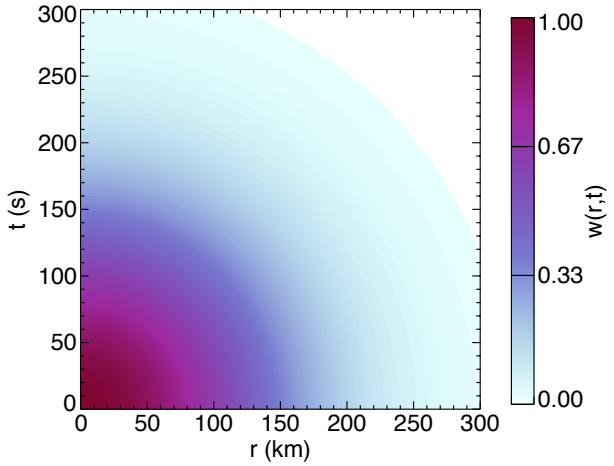

Figure 3: Contour plot of the space-time weighting applied to NEXRAD WSR-88D Level 2 observations in the GridRad binning procedure.

Step 4. Bin radar variable(s) scaled by space-time weights into common grid.

The final step of the GridRad algorithm involves merging multiple observations of a given radar variable into the common grid volumes (i.e., 'bins') of the GridRad domain. In the Level 2 data, each radar volume on the polar grid is flagged to indicate whether a valid measurement was made and whether echo was detected. The value of a radar variable V on the GridRad grid is equal to the weighted average of all observations in which echo was detected

$$V(x_i, y_j, z_k) = \frac{\sum_{n=1}^{N_{\text{echo}}} w_n \, v_n}{\sum_{n=1}^{N_{\text{echo}}} w_n} \, , \tag{3}$$

where N_{echo} is the number of Level 2 radar volumes with echo that contribute to the grid volume at location (x_i, y_j, z_k), $w_n = w(r_n, t_n)$ is the space-time weight of the nth Level 2 radar volume on its polar grid (from Equation 2 and Figure 3 above), and v_n is the value of the observed radar variable for the nth Level 2 radar volume. The total weight W is

$$W(x_i, y_j, z_k) = \sum_{n=1}^{N_{\text{echo}}} w_n \, . \tag{4}$$

Thus the GridRad data are averages conditioned on whether echo is observed. Though generally advantageous for all radar variables, this space-time weighting approach is especially beneficial for estimating polarimetric variables, which can be significantly degraded at far ranges where the minimum detectable Z_{H} increases and the signal-to-noise ratio becomes small. Prescribing less weight to distant scans with potentially degraded data quality mitigates possible detrimental effects on the resulting GridRad analysis.

The result of the binning process is two parameters for each radar variable: the weighted average V (e.g., Z_{H}) and the sum of the weights W. Two additional parameters that are useful for post-processing quality control are also archived: N_{obs}, which is the number of valid Level 2 radar volumes that observed each GridRad volume (with or without echo), and N_{echo}. W is also useful for quality control as it represents a measure of the intrinsic resolution and/or sampling within a given GridRad volume. Since the space and time resolution of the Level 2 spherical grids (and ultimately, the number of gates that can be merged) varies over time, the weights indicative of a well-sampled GridRad volume are $\sim$0.33 prior to the NEXRAD WSR-88D upgrade to super-resolution in 2008 and $\sim$1.0 thereafter (not shown, but based on a large number of comparisons with higher-resolution observations - e.g., see Figs. 4 and 5 here).

4 Data Quality

The gridded radar variables output by the GridRad procedure have some intrinsic characteristics and limitations set by the original scales of the contributing NEXRAD WSR-88D Level 2 gates, the availability of data, common artifacts present in the observations, and the gridding procedure employed. For brevity, an outline of the expected resolution of the data and a description of the most common sources of error are provided in the following subsections.

4.1 Resolution

As discussed at various points in Sections 2 & 3 above, individual grid volumes (or gates) in NEXRAD Level 2 data exist at a resolution of $\Delta r \times \ell(r)^2$, where $\ell(r)$ is the beam width/depth as a function of range. For observations that carry the vast majority of weight in GridRad output (i.e., see Fig. 3), these grid volumes are 1 km $\times$ ($\leq$3)^2 km^2 in observations prior to 2008 and 0.25 km $\times$ ($\leq$3)^2 km^2 in observations following the super-resolution upgrade. Though the finer horizontal dimension of the observations is $\leq$1 km, the process of merging involves collecting data from multiple viewing angles at a point and averaging them together. Such a process leads to a loss of information at the finest resolved scales (i.e., smoothing), a reduction in noise (error), and a mean resolution similar to the larger dimension of the Level 2 radar volume (for NEXRAD WSR-88D observations this is the cross-beam dimension $\ell(r)$, except when r is small). The potential loss of information is one of the main motivating factors for applying distance-weighting to contributing observations in a multi-radar dataset. Weighting observations from nearby radars higher than those from distant radars preserves the higher resolution data. Given the rapid decrease in space-time weight as a function of range applied to Level 2 gates in the GridRad procedure, the gridded radar variables produced are expected to have an average horizontal resolution similar to the common grid spacing: $\sim$2 km.

Vertical resolution of GridRad data is primarily influenced by two factors: 1) the combined vertical sampling from neighboring radars, and 2) the beam depth $\ell(r)$. The combined vertical sampling and coverage within the NEXRAD WSR-88D network is greatest (typically $\sim$0.5 to 1 km, depending on VCP of contributing radars; see Fig. 2) where the mean range of a grid point from contributing radars is $\sim$130 km, which corresponds to an average beam depth of $\sim$2 km. As a result, the combined vertical sampling from multiple radars typically exceeds the native resolution of Level 2 gates by a factor of two or more. Given this characteristic and the strict 1.5 km contributing depth limit of a Level 2 gate in Step 2 of the GridRad procedure, the gridded radar variables produced are expected to have an average vertical resolution of 1-2 km, also similar to the vertical spacing of the common grid (1 km).

To better demonstrate these expected resolutions of the GridRad data, two example data comparisons with observations from similar systems made at finer spatiotemporal resolution are provided here. For both comparisons, the GridRad data have been quality controlled using the recommended methods outlined in Section 5.1 below. First, a comparison with 1-minute observations taken by a vertically pointing S-band radar operated during the Midlatitude Continental Convective Clouds Experiment is shown (MC3E; Jensen et al., 2016). Four NEXRAD radars contribute to the GridRad data at the location of the MC3E radar, made at distances of about 60, 120, 140, 180 km from their locations. Figure 4 shows vertical time curtains of Z_{H} from the MC3E observations and from GridRad data over a time period of 17.5 hours. The MC3E data are shown i) in their native form (an altitude resolution Δz of 62.5 m; Fig. 4a) and ii) following altitude (2-km running mean) and time ($\pm$4-min Gaussian) smoothing in an effort to mimic the GridRad binning procedure (Fig. 4c). Note that there are some scanning artifacts at and above the echo top in the MC3E data, mostly prior to 400 minutes past 00:00 UTC. This comparison reveals two important characteristics of the GridRad data. First, the finer vertical resolution of the MC3E data is clear, with the Z_{H} maximum

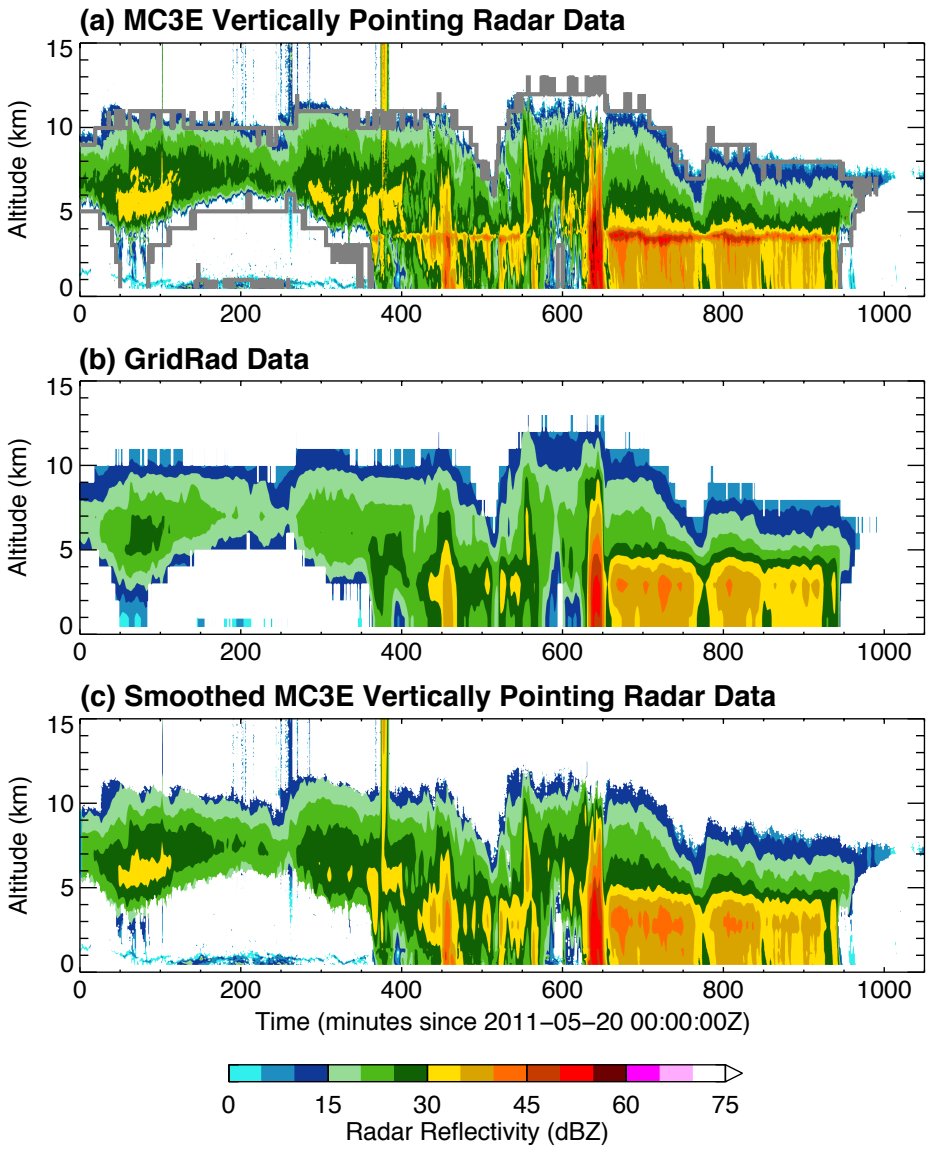

Figure 4: Vertical time curtains of Z_{H} from (a) a vertically pointing S-band Doppler radar stationed at the DOE-ARM measurement site in Lamont, Oklahoma during MC3E, (b) GridRad data created at equivalent time resolution, and (c) vertically pointing S-band radar data smoothed in altitude and time at scales consistent with the GridRad procedure. These observations were taken from 00:00 to 17:30 UTC on 20 May 2011. The GridRad echo boundary is superimposed in (a) to enable direct comparison (gray line).

coincident with the melting level (the so-called "bright band") well-defined in stratiform rain regions in the MC3E data and less defined in the GridRad data (e.g., between altitudes of 3 and 4 km prior to 550 min and after 650 min). The magnitude of Z_{H} is also commonly ∼5 dBZ lower in GridRad data, though such differences are largely reduced if the MC3E data is smoothed to emulate the GridRad binning procedure. Furthermore, remaining differences following smoothing of the MC3E data would likely be reduced further if the intrinsic horizontal smoothing of GridRad data could be reproduced (this is impossible because the MC3E data is a point measurement). Second, though differences in Z_{H} are apparent, the echo boundaries (e.g., echo top and bottom) are comparable between the two datasets. The contributing depth restriction imposed during Step 2 of the GridRad procedure is largely responsible for such agreement.

The second dataset comparison provided here demonstrates the potential for multi-sensor analyses using GridRad data and similar datasets from space-based sensors obtained at higher space and time resolution. In particular, Figure 5 shows vertical profiles taken by the Cloud-Aerosol Lidar with Orthogonal Polarization (CALIOP) aboard the CALIPSO satellite (Winker et al., 2009) and the Cloud Profiling Radar (CPR) aboard the CloudSat satellite (Stephens et al., 2002), both of which operate in close succession within the shared orbit of the NASA Afternoon constellation of satellites (or A-Train). The GridRad data shown in this example were created at the satellite overpass times. The differences in the spatial resolution of these datasets is clear, given that the CALIOP data is obtained at a spatial resolution of 335–1000 m $\times$ 30–60 m ($\Delta x \times \Delta z$) and the CPR data is obtained at a spatial resolution of 1.1 km $\times$ 240 m ($\Delta x \times \Delta z$). The combined sampling of all three systems, however, demonstrates that the GridRad data: i) provide Z_{H} echo top altitudes that are consistent with the CloudSat CPR (see also Fig. 6), and ii) help to fill in the depth of the cloud that is not well sampled by CALIOP and CPR, given that both satellite-based sensors suffer from attenuation in volumes with large precipitation-sized particles.

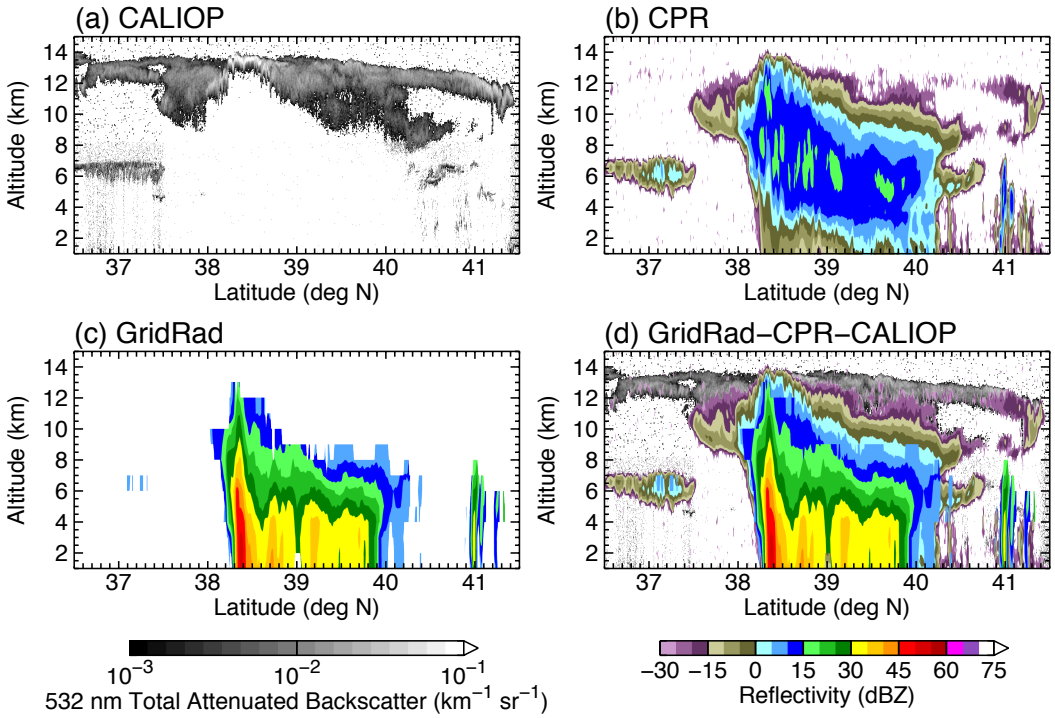

Figure 5: For a CONUS overpass by the A-Train on 8 June 2015 from 0808 to 0810 UTC: (a) CALIOP 532 nm total attenuated backscatter, (b) CloudSat CPR radar reflectivity, (c) GridRad radar reflectivity Z_{H}, and (d) an overlay of all three datasets.

4.2 Limitations

In addition to the limitations of spatial resolution and frequency of the available GridRad data, one of the most important limitations users should consider is the minimum detectable Z_{H}. NEXRAD WSR-88D radars are capable of sensing Z_{H} well below the scale of dense precipitable hydrometeors, especially at close ranges from the radar. The minimum detectable signal of the radar is -42 dBZ at 1 km and increases with increasing range to about 11 dBZ at the maximum detectable range of 460 km (Crum and Alberty, 1993). For the observations merged in the GridRad procedure (i.e., those within 300 km of each radar), the

minimum detectable $Z_{\mathrm{H}} \leq 7.5$ dBZ. Thus, data merged into the GridRad domain can span a wide range of Z_{H}, especially considering that the maximum observed Z_{H} in storms over the CONUS is about 80 dBZ. Nevertheless, the vast majority of Z_{H} in GridRad is $\geq$5 dBZ.

Apart from the obvious limitations related to resolution, sampling, Level 2 data availability, and the temporal availability of the public GridRad dataset outlined above, there are sources of error in the native NEXRAD WSR-88D Level 2 observations that propagate into the GridRad data (i.e., artifacts that are not removed during the 4-step GridRad procedure) which users should expect to encounter. Short descriptions of such error are provided below, with discussion limited to the most common errors. Many of these errors can be largely mitigated through use of the available quality control routines discussed in Section 5 below.

One of the most common sources of error in radar observations is non-standard beam refraction (commonly referred to as 'anomalous propagation' or AP). As outlined in Section 3 above, the altitude of each beam in a radar volume used for binning in the GridRad procedure is calculated assuming a standard index of refraction for the atmosphere. Under dry, near-adiabatic conditions in the lower atmosphere, radar beams can refract less than expected and result in an underestimation of the true beam altitude for binning. Conversely, over-estimation of the radar beam altitude is possible if the beam refracts more than expected, which is common if there are significant temperature inversions in the tropospheric boundary layer. These errors from non-standard refraction, however, are typically limited to beams that travel long distances in the boundary layer (e.g., Doviak and Zrnić, 1993). A correction for this source of error does not exist in the provided GridRad quality control routines.

Contamination of the radar measurement from beam side lobes is also a common source of error in radar observations, but is relatively rare at Z_{H} observed within the GridRad data. In general, side lobe contamination is only possible from the first lobe, -27 dBZ below the main lobe power for a NEXRAD WSR-88D radar and at 1.2 degrees away from the beam center in all directions (up to 6 km in altitude for ranges within 300 km). In order for side lobe contamination to be present, the Z_{H} of the scatterer in the path of the side lobe must be stronger than the signal in the path of the main lobe by at least the two-way, first-side lobe isolation (i.e., $\geq$54 dBZ, OFCM, 2005). At the typical 5 dBZ minimum of Z_{H} in GridRad data, side lobe contamination of a given beam requires that Z_{H} within 1.2 degrees of the beam center exceed 59 dBZ. A correction for this source of error is possible using the provided GridRad quality control routines.

The sun emits radiation at all wavelengths. During sunrise and sunset, NEXRAD WSR-88D radars may receive such radiation within beams coincident with the sun's inclination, leading to Z_{H} typically less than 20 dBZ that is confined to a few azimuthal samples at a single elevation. Such radar signals are commonly referred to as 'sun strobes' and are observed when clouds are not present along the line of sight to the sun. This error is almost entirely mitigated using the provided GridRad quality control routines. Note that sun strobes are somewhat analogous to interference detected from microwave transmitters near the WSR-88D radars, which can be a more persistent source of error, but is also well-mitigated using the provided GridRad quality control routines.

5 Example Code and GridRad Data Usage

To enable easy access and use of the GridRad data, we have provided sample read and quality control routines written in the *IDL* (*Interactive Data Language*) and *Python* programming languages. Table 2 lists these routines and their utility.

Procedure Name (language)	**Input**	**Purpose**
`gridrad_read_file` (IDL) `gridrad.read_file` (Python)	Full path to location of GridRad file.	Read contents of GridRad file.
`gridrad_filter` (IDL) `gridrad.filter` (Python)	GridRad data structure from gridrad_read_file.	Remove observations with low echo frequency or W.
`gridrad_remove_clutter` (IDL) `gridrad.remove_clutter` (Python)	GridRad data structure from gridrad_read_file.	Remove echo that is objectively flagged as non-meteorological.

Table 2: Name, input, and purpose of provided code to read and quality control the GridRad data. The IDL code is provided as three separate procedures with file names that match the procedure names (with a '.pro' file extension). The Python programs are provided as a single file ('gridrad.py').

To reduce file size, the GridRad data files use a combination of a sparse storage scheme and internal netCDF-4 file compression. The file reading programs return full, three-dimensional arrays of GridRad data to the user. Filtering and decluttering options are discussed in the following section.

5.1 Recommendations

The GridRad data provided in the public archive contain the raw outputs of the 4-step GridRad procedure. The data are built using every available successful NEXRAD WSR-88D Level 2 observation, including those with possible artifacts or non-meteorological scatter.[2] Thus, for users who aim to study and/or evaluate high-quality meteorological echo, it is recommended that two quality control techniques be applied to the data prior to analysis. First, many low-quality observations and scanning artifacts can be removed by evaluating the frequency at which echo is present within all available NEXRAD observations (referred to here as 'filtering'). This is the central idea behind the `gridrad_filter` programs, which identify GridRad volumes with low W (the precise threshold depends on the magnitude of Z_{H} and, due to changes in NEXRAD sampling, the date of the observation) or low echo frequency ($N_{echo}/N_{obs} < 0.6$, if $N_{obs} \geq 3$) and removes the binned radar variables (sets them equal to a not-a-number). The goal of this filtering approach is to retain echo that has either been observed consistently from multiple Level 2 volumes or was made in close proximity to a contributing radar and close in time to that of the GridRad analysis. To demonstrate the benefit of filtering, we provide an example analysis comparing Z_{H} = 5 dBZ echo top altitudes computed using GridRad data and higher-resolution CloudSat CPR data in Figure 6. This comparison shows that 5-dBZ echo top altitudes based on the raw GridRad data are biased nearly 1 km high, those based on the recommended N_{echo}/N_{obs} filtering threshold of 0.6 are nearly unbiased, and those based on the highest possible threshold of 1.0 (or 100%) are biased nearly 1 km low. Thus, we recommend that GridRad data used for meteorological studies be filtered.

The `gridrad_remove_clutter` programs are designed to remove non-meteorological echo from biological scatterers and artifacts such as noisy returns or 'speckles.' The approaches employed are largely modeled after the ideas outlined in Zhang et al. (2004) for native NEXRAD WSR-88D Level 2 volumes.

[2] A small number of Level 2 volume scans (∼425 volume scans in 325 analyses) with known quality problems have been excluded from GridRad analyses in the public archive.

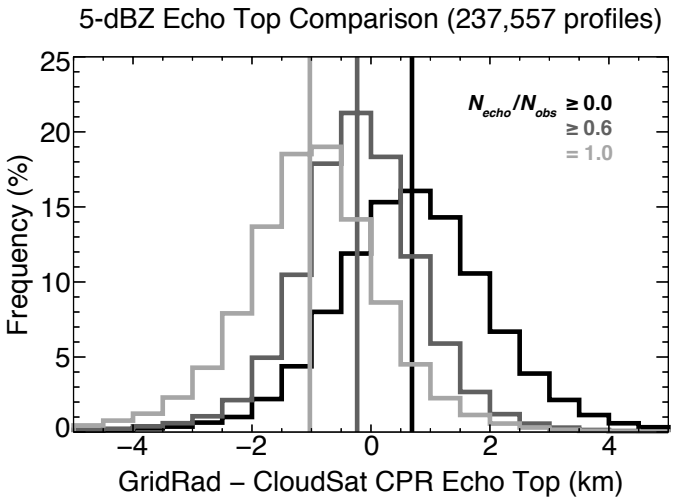

Figure 6: Frequency distributions of Z_{H} = 5 dBZ echo top altitude differences between those diagnosed using GridRad data and those from higher-resolution CloudSat Cloud Profiling Radar (CPR) observations. Distributions are shown for echo frequency thresholds N_{echo}/N_{obs} of 0.0 (black), 0.6 (dark gray), and 1.0 (light gray). This comparison is based on 237,557 observed Z_{H} profiles between 2006 and 2016.

First, GridRad volumes containing echo are checked for additional echo in immediately adjacent volumes at the same altitude. If the total echo coverage in the neighboring grid volumes (and the volume in question) is less than 32%, the reflectivity is changed to a missing value. Second, GridRad columns with weak echo that is contained entirely within the lowest altitude levels are removed. This second step will remove some meteorological echo in shallow precipitation (mostly winter storms) and thus is optional in the `gridrad_remove_clutter` routine. Third, non-meteorological echo below the anvils of deep convection is removed. This step requires a layer of echo-free GridRad volumes between the anvil in the upper troposphere and (mostly biological) scatter in the tropospheric boundary layer. Last, a second check for sufficient echo coverage is applied that is equivalent to the first step. It is recommended that the full 4-step clutter removal process be used for analysis of deep cloud systems and that shallow echo removal (the optional step 2) not be used for shallow cloud systems.

Figure 7 shows column-maximum Z_{H} from an example GridRad analysis with all possible combinations of quality control applied. This analysis time has multiple precipitation regimes, with a shallow cold rain system over northern Illinois and southeastern Wisconsin and a deeper mesoscale convective system ahead of a cold front and in the warm sector of an extratropical cyclone (over Alabama, Tennessee, and Kentucky). In the raw data, biological scatterers are present over the eastern U.S. and sun strobes occur over the central plains (extending west of contributing radars since this analysis time is near sunset). These non-meteorological echoes are effectively removed through application of one or more of the possible combinations of quality control techniques. Partial removal of the shallow cold rain system does occur in this example when the full clutter removal method is applied, as discussed above.

5.2 GridRad Examples of Common Radar Analyses

The GridRad data enable novel analyses of observed clouds and precipitation over the CONUS. Potential uses of the data include evaluating and testing convective parameterizations in global climate models as well as resolved convection simulated by non-hydrostatic models, validating satellite methods that are used in re-

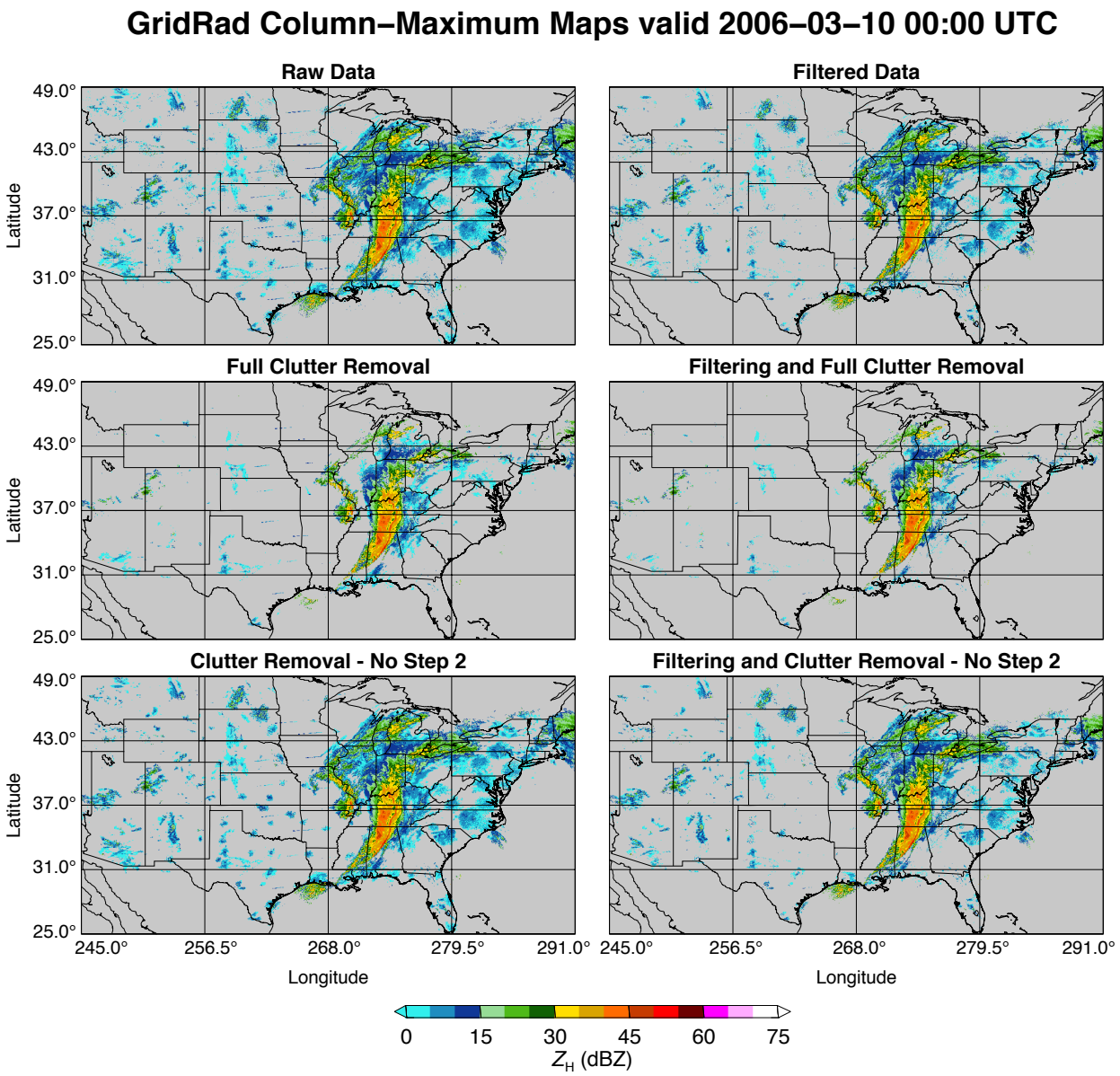

Figure 7: Maps of GridRad column-maximum Z_H with and without all possible combinations of the provided quality control techniques. The GridRad analysis is valid 10 March 2006 at 00:00 UTC.

gions without a dense radar network, and climatological studies of precipitating systems in the extratropics to advance our understanding of a range of meteorological, climatological, and hydrological processes. To provide users with some insight into these possibilities, examples of common radar analyses with GridRad data are presented here. These examples were produced using the *GridRad Viewer* software developed by C. Homeyer in *IDL* and made available online at GridRad.org. The full recommendations for quality control were applied to the GridRad data used in these examples.

Figure 8 shows maps of GridRad data and derived products for a subdomain of the 00:00 UTC analysis on 1 May 2010 that is available in the public archive. In this analysis, deep convection is present over northeast Texas, Arkansas, and southeast Missouri, with shallower storms covering most of the Florida pan-

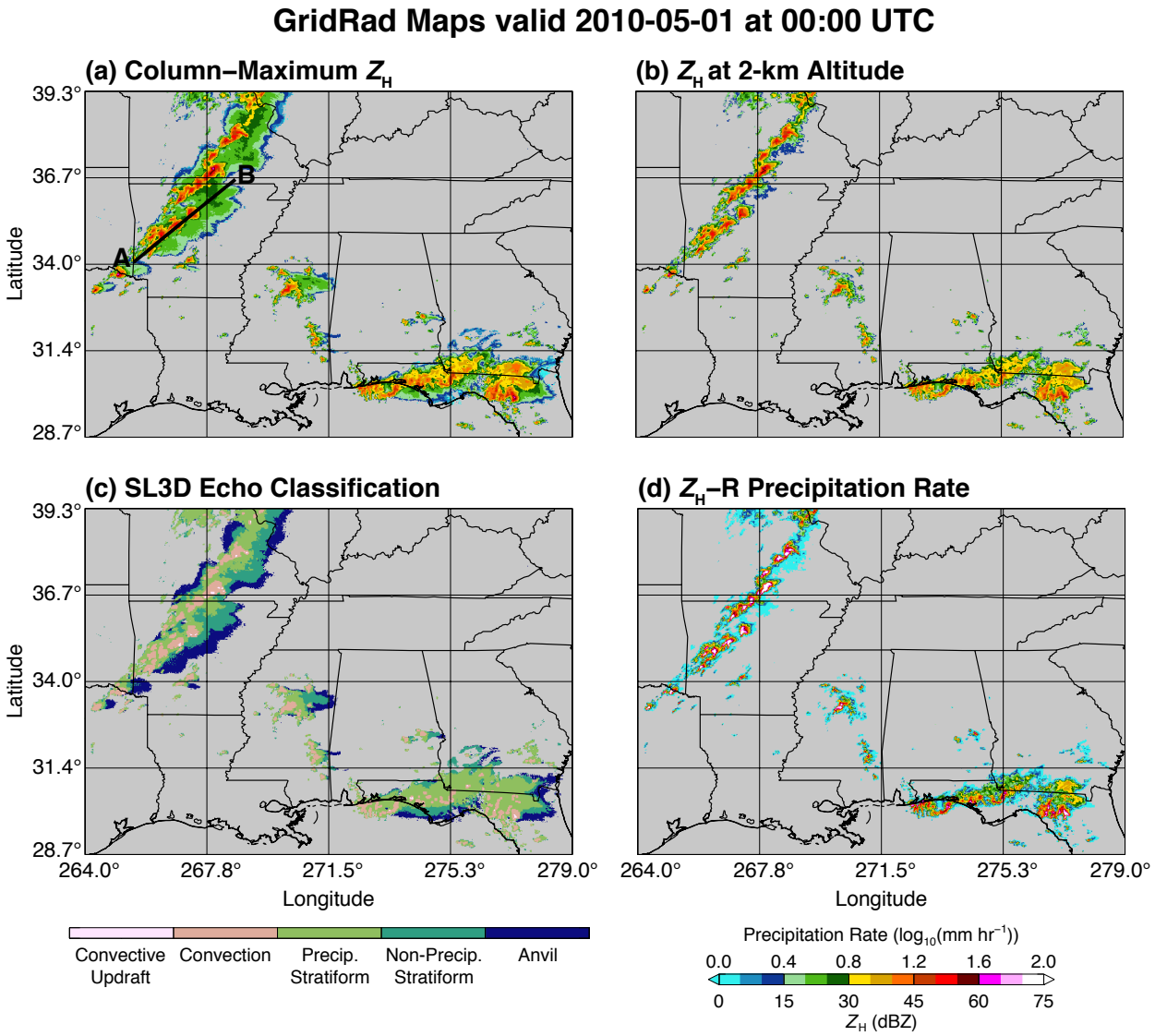

Figure 8: For the hourly GridRad analysis valid at 00:00 UTC on 1 May 2010, maps of (a) column-maximum Z_H, (b) Z_H at an altitude of 2 km, (c) Z_H echo classification from the Storm Labeling in 3 Dimensions (SL3D) algorithm, and (d) rain rates computed using a Z_H–R power law relationship. The thick black line labeled 'A–B' in (a) represents the path of the vertical cross-section provided in Fig. 9.

handle. Figures 8a and 8b show column-maximum Z_H and Z_H at a constant altitude of 2 km, respectively, revealing areas of precipitation and related echo aloft (non-precipitating cloud, some being anvil produced by deep convection). In many radar-based studies of clouds and precipitation, investigators seek to separate regions where the precipitation is generated by convective or stratiform growth processes. Figure 8c shows such a separation, via an echo classification algorithm named the Storm Labeling in 3 Dimensions algorithm (SL3D; Starzec et al., 2017), which was recently developed using GridRad data. The SL3D algorithm classifies echo into 5 categories: convection, convective updraft, precipitating stratiform, non-precipitating stratiform, and anvil. The results of the SL3D classification for this case are consistent with what one would infer from comparing the Z_H maps in Figs. 8a and 8b. Finally, Figure 8d shows rain rate estimates calculated from Z_H using a power law relationship (a so-called "Z–R" correlation, e.g., Marshall and Palmer, 1948; Battan, 1973; Jorgensen and Willis, 1982). In this case, unique empirical $Z_H - R$ relationships, where R is

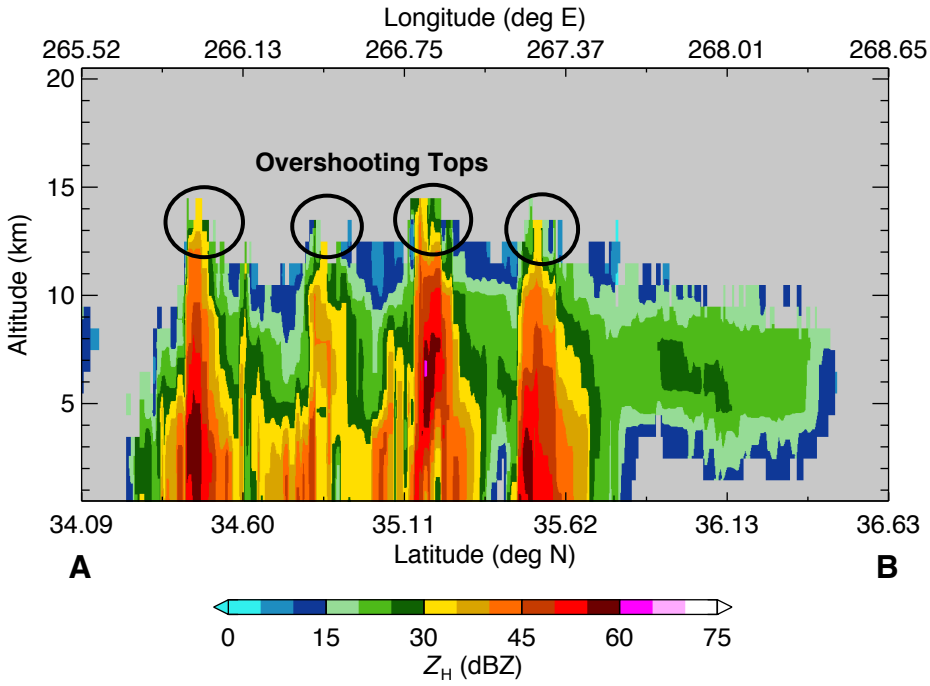

Figure 9: Vertical cross-section of Z_{H} along the line labeled 'A–B' in Fig. 8a. Echo within convection extending above the broader echo top (i.e., "overshooting tops") is identified by the black ellipses.

used as the discriminant, are applied to convective $\left(Z_{\mathrm{H}} = 300R^{1.4}\right)$ and stratiform $\left(Z_{\mathrm{H}} = 75R^{2}\right)$ regions, which are identified using the SL3D classification from Figure 8c. Here, the rain rate is computed using the Z_{H} at the lowest observed altitude within the 1–3 km ASL layer since the lowest altitude at which a GridRad column is observed varies depending on radar coverage in the CONUS (e.g., see Fig. 1). Note that Z_{H} is in units of $\mathrm{mm}^6\ \mathrm{m}^{-3}$ for these rain rate calculations.

Many studies of radar observations involve evaluating the vertical structure of storms. Figure 9 shows a vertical cross-section of Z_{H} taken along the path labeled 'A–B' in Fig. 8a and bisecting the deep convection over Arkansas. Elements of at least four individual convective cores are evident in this vertical cross-section, each of which is reaching altitudes 1 to 3 km above the neighboring stratiform and anvil regions. These convective features are typically referred to as "overshooting tops" and are identified by the black ellipses in Figure 9. A common alternative approach to evaluating the vertical structure of radar echo is through the use of a statistical Contoured Frequency by Altitude Diagram (CFAD; Yuter and Houze, 1995). Figure 10 presents a CFAD of Z_{H} for all echo classified as convection or convective updraft by the SL3D algorithm within the domain of Figure 8. This CFAD is consistent with previous evaluations of convection in the literature and also reveals the presence of overshooting tops in this GridRad analysis.

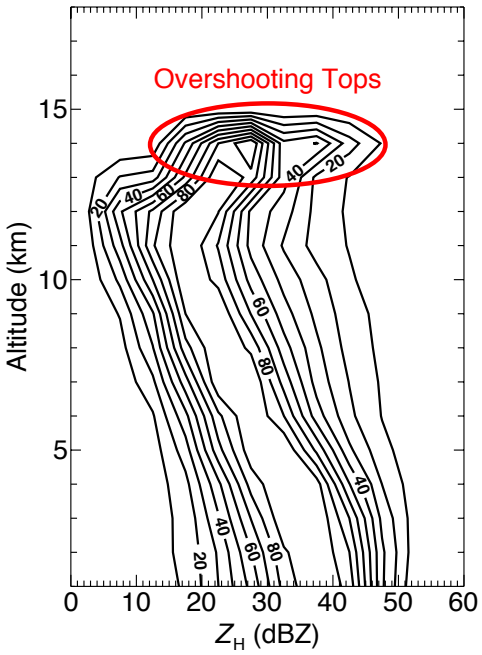

Figure 10: A Contoured Frequency by Altitude Diagram (CFAD) of Z_{H} within regions classified as convection or convective updraft by the Storm Labeling in 3 Dimensions (SL3D) algorithm shown in Fig. 8. The overshooting tops identified in Fig. 9 are identified here (within the red ellipse) as a shift of the distribution to higher Z_{H} at the highest altitudes where echo was observed.

6 Table of Symbols

Symbol	Units and/or numerical value	Quantity
Z_{H}	dBZ	radar reflectivity at horizontal polarization
V_{R}	m s^{-1}	radial velocity from Doppler shift
σ_{V}	m s^{-1}	velocity spectrum width
Z_{DR}	dB	differential radar reflectivity
ϕ_{DP}	$^{\circ}$	differential propagation phase shift
ρ_{HV}	dimensionless	co-polar correlation coefficient
L	150 km	spatial weighting scale
τ	150 s	temporal weighting scale
r	km	radial distance from the radar
Δt	s	time difference between observation and analysis
x, x_i	$^{\circ}$E	longitude
y, y_j	$^{\circ}$N	latitude
z, z_k	km	altitude with respect to the geoid
w_i	dimensionless	weight for a single radar observation
W	dimensionless	total weight
v_i		single observation of a radar variable
V		weighted average of a radar variable
N_{obs}	dimensionless	number of observations in GridRad volume
N_{echo}	dimensionless	number of observations with echo in GridRad volume
Δx	km	horizontal resolution
Δz	km	altitude resolution
Δr	km	radial resolution of Level 2 observation
ℓ	km	radar beam width or depth
R	mm hr^{-1}	rain rate

7 References Cited

Battan, L. J., 1973: *Radar Observations of the Atmosphere*, 324 pp. The University of Chicago Press.

Crum, T. D. and R. L. Alberty, 1993: The WSR-88D and the WSR-88D operational support facility. *Bull. Amer. Meteorol. Soc.*, **74 (9)**, 1669–1687.

Doviak, R. J. and D. S. Zrnić, 1993: *Doppler Radar and Weather Observations*. 2d ed., ISBN 0-486-45060-0, Dover Publications, Inc., 31 East 2nd Street, Mineola, NY, 11501.

Homeyer, C. R., 2014: Formation of the enhanced-v infrared cloud top feature from high-resolution three-dimensional radar observations. *J. Atmos. Sci.*, **71**, 332–348, doi:10.1175/JAS-D-13-079.1.

Jensen, M. P., et al., 2016: The Midlatitude Continental Convective Clouds Experiment (MC3E). *Bull. Amer. Meteorol. Soc.*, **97**, 1667–1686, doi:10.1175/BAMS-D-14-00228.1.

Jorgensen, D. P. and P. T. Willis, 1982: A Z-R relationship for hurricanes. *J. Appl. Meteor.*, **21**, 356–366.

Langston, C., J. Zhang, and K. Howard, 2007: Four-dimensional dynamic radar mosaic. *J. Atmos. Oceanic Technol.*, **24**, 776–790, doi:10.1175/JTECH2001.1.

Marshall, J. S. and W. M. Palmer, 1948: The distribution of raindrops with size. *J. Meteorol.*, **5**, 165–166.

OFCM, 2005: Federal Meterological Handbook No. 11 – Doppler Radar Meteorological Observations, Part B: Doppler Radar Theory and Meteorology. FCM-H11B-2005 (Available online at http://www.ofcm.gov/publications/fmh/allfmh2.htm).

OFCM, 2006: Federal Meterological Handbook No. 11 – Doppler Radar Meteorological Observations, Part C: WSR-88D Products and Algorithms. FCM-H11C-2006 (Available online at http://www.ofcm.gov/publications/fmh/allfmh2.htm).

Starzec, M., C. R. Homeyer, and G. L. Mullendore, 2017: Storm Labeling in 3 Dimensions (SL3D): A volumetric radar echo and dual-polarization updraft classification algorithm. *Mon. Wea. Rev.*, **145**, 1127–1145, doi:10.1175/MWR-D-16-0089.1.

Stephens, G. L., et al., 2002: The CloudSat mission and the A-Train. a new dimension of space-based observations of clouds and precipitation. *Bull. Amer. Meteorol. Soc.*, **83**, 1771–1790, doi:10.1175/BAMS-83-12-1771.

Trapp, R. J. and C. A. Doswell, 2000: Radar data objective analysis. *J. Atmos. Oceanic Technol.*, **17**, 105–120.

Winker, D. M., M. A. Vaughan, A. Omar, Y. Hu, K. A. Powell, Z. Liu, W. H. Hunt, and S. A. Young, 2009: Overview of the CALIPSO mission and CALIOP data processing algorithms. *J. Atmos. Oceanic Technol.*, **26**, 2310–2323, doi:10.1175/2009JTECHA1281.1.

Yuter, S. E. and R. A. Houze, 1995: Three-dimensional kinematic and microphysical evolution of Florida cumulonimbus. part ii: Frequency distributions of vertical velocity, reflectivity, and differential reflectivity. *Mon. Wea. Rev.*, **123**, 1941–1963.

Zhang, J., K. Howard, and J. J. Gourley, 2005: Constructing three-dimensional multiple-radar reflectivity mosaics: Examples of convective storms and stratiform rain echoes. *J. Atmos. Oceanic Technol.*, **22**, 30–42.

Zhang, J., S. Wang, and B. Clarke, 2004: WSR-88D reflectivity quality control using horizontal and vertical reflectivity structure. *11th Conf. on Aviation, Range, and Aerospace Meteorology*, Amer. Meteor. Soc., P5.4.